NJC

PAPER

View Article Online
View Journal | View Issue

Cite this: *New J. Chem.*, 2016, **40**, 5885

Coordination compounds of a hydrazone derivative with Co(III), Ni(II), Cu(II) and Zn(II): synthesis, characterization, reactivity assessment and biological evaluation†

B. Barta Holló,[a] J. Magyari,[a] S. Armaković,[b] G. A. Bogdanović,[c] M. V. Rodić,[a] S. J. Armaković,[a] J. Molnár,[d] G. Spengler,[d] V. M. Leovac[a] and K. Mészáros Szécsényi*[a]

A new hydrazone-type ligand with a five N-donor set and its coordination compounds with Co(III), Ni(II), Cu(II) and Zn(II) metal centres were synthesized. The crystal and molecular structure of the Co(III) complex was determined by X-ray structural analysis. All the compounds were characterized by elemental analysis, molar conductivity and FT-IR spectral data. The cobalt(III) compound is a neutral binuclear complex formed by coordination of two, doubly deprotonated ligand anions as bridges between the Co(III) centres. The metal centres are additionally connected by a peroxido bridge, which was observed for the first time in Co(III) complexes with similar ligands. The other coordination compounds are mononuclear complexes wherein only one doubly deprotonated ligand is coordinated to the central ion in a tetradentate fashion. The structures were theoretically investigated employing density functional theory (DFT) calculations with B3LYP exchange–correlation functional and LACV3P+(d,p) basis sets for the coordination compounds and 6-31+G(d,p) basis set for the ligand. Molecular electrostatic potential (MEP) and average local ionization energy (ALIE) surfaces were calculated to study the reactive properties of the compounds. The thermal behaviour of the compounds was determined by simultaneous thermogravimetric-differential scanning calorimetric (TG-DSC) measurements and the results were correlated to the proposed structures and to calculated MEP/ALIE surfaces. The compounds were tested *in vitro* for antiproliferative effects on parental (L5178Y) mouse T-cell lymphoma cells, on L5178Y transfected with pHa ABCB1/A retrovirus and for reversal of multidrug resistance (MDR) in tumor cells by flow cytometry. The preliminary measurements showed that the cobalt(III) compound was an effective inhibitor of the ABC transporter PGP drug efflux pump. The ligand was somewhat less effective, the zinc complex had a moderate inhibition activity, whereas the nickel(II) and copper(II) compounds were inactive.

Received (in Victoria, Australia) 19th February 2016,
Accepted 26th April 2016

DOI: 10.1039/c6nj00560h

www.rsc.org/njc

Introduction

Cancer mortality accounts for about one eighth of all deaths in the world. During the past 30 years, the annual cancer incidence has doubled. Around 1.5 million new cancer cases and 0.6 million cancer deaths are projected to occur in the United States in 2015.[1] Carcinogenesis underlies complex mechanisms and to address single target approaches is inadequate to prevent prevalence and deaths from the disease. Adjuvant therapy of cancer may decrease the development of drug resistance to some extent. However, multidrug resistance (MDR) caused by specific membrane transporters, such as ATP-binding cassette (ABC) or copper transporters, as well as other causes of drug resistance, hamper successful cancer chemotherapy.[2]

Numerous pyridazine derivatives are biologically active. In addition to the natural products with pyridazine, a high number of synthetic derivatives are in use as pharmaceuticals for treatment of inflammations, pain, enzyme dysfunctions and tumors.[3a–d] For more than ten years, Dal Piaz *et al.* studied the pyridazine derivatives with antinociceptive activity.[4a,b] Pyridazine-type vasodilators are

[a] *University of Novi Sad, Faculty of Sciences, Department of Chemistry, Biochemistry and Environmental Protection, Trg Dositeja Obradovića 3, 21000, Novi Sad, Serbia. E-mail: mszk@uns.ac.rs*
[b] *University of Novi Sad, Faculty of Sciences, Department of Physics, Trg Dositeja Obradovića 4, 21000, Novi Sad, Serbia*
[c] *"Vinča" Institute of Nuclear Sciences, Laboratory of Theoretical Physics and Condensed Matter Physics, University of Belgrade, P.O. Box 522, 11001 Belgrade, Serbia*
[d] *University of Szeged, Faculty of Medicine, Department of Medical Microbiology and Immunobiology, Dóm tér 10, H-6720 Szeged, Szeged, Hungary*

† Electronic supplementary information (ESI) available. CCDC 1432904 (**1**). For ESI and crystallographic data in CIF or other electronic format see DOI: 10.1039/c6nj00560h

also described.[5a,b] The relatively simple structure and high reactivity of pyridazines make them good candidates for synthesis of more complex heterocyclic systems. The coordination chemistry of pyridazine-based compounds is sparsely covered and mainly focused towards selected heavy metals[6a–e] although they are suitable for coordination complex formation.[7a,b] The activity of biologically active compounds can be modified by coordination to transition metal ions.[8a–c] Sometimes the activity of the ligand is increased by its coordination,[9a,b] but the opposite effect is also observed.[10] Schiff base-type ligands and their coordination compounds display a wide spectrum of biological activity ranging from antimicrobial effect[11] and cytotoxicity against various cancer cells.[12a,b]

The reaction between 3-chloro-6-hydrazinopyridazine (Hp) with 2,6-diacetylpyridine results in the formation of a new potentially pentadentate Schiff base-type ligand bis(3-chloropyridazine-6-hydrazon)-2,6-diacetylpyridine (**Hp_2DAP**). We present herein the synthesis, structural and physicochemical properties of the **Hp_2DAP** ligand and its complexes with Co(III), Ni(II), Cu(II) and Zn(II) metal centres, $[Co_2(\mu\text{-}Hp_2DAP\text{-}2H)_2(\mu\text{-}O_2)]\cdot 4H_2O$ (**1**), $[Ni(Hp_2DAP\text{-}2H)]$ (**2**), $[Cu(Hp_2DAP\text{-}2H)]\cdot H_2O$ (**3**) and $[Zn(Hp_2DAP\text{-}2H)]\cdot H_2O$ (**4**), respectively. Density functional theory (DFT) calculations were performed on all the compounds and the molecular electrostatic surfaces (MEP) and average local ionization energy (ALIE) surfaces were calculated to determine the reactivity centres. The compounds were tested with resistance modifier steroid compounds to overcome drug resistance in resistant human ABCB1-expressing mouse lymphoma cells. The structural data and the calculated MEP and ALIE surfaces were correlated to understand the thermal properties and the biological activity of the compounds.

Experimental

Synthesis of the compounds

Hp_2DAP. After dissolving 5 mmol (0.726 g) of 3-chloro-6-hydrazinopyridazine (Hp) in 10 cm^3 acetonitrile under reflux at 60 °C, 2.5 mmol (0.410 g) of 2,6-diacetylpyridine (DAP) dissolved in 5 cm^3 acetonitrile was added. The reaction mixture was diluted by 2 cm^3 acetonitrile and the reflux continued for 30 min at 60 °C. A light orange amorphous precipitate was filtered after 24 h, washed with acetonitrile and dried in air at room temperature. Yield: 93.6%, M_r = 416.27 (found: C, 49.1; H, 3.6; N, 30.3, calc. for $C_{17}H_{15}Cl_2N_9$ C, 49.10; H, 3.82; N, 30.00%). λ_M (S cm^2 mol^{-1}) = 0.74.

The coordination compounds were prepared by the following general procedure:

The ligand, **Hp_2DAP** (0.25 mmol, 0.104 g) was suspended in 15 cm^3 methanol by heating and intensive stirring. To the warm suspension, a warm solution of Co(II), Ni(II) or Cu(II) acetate (0.25 mmol) in 5 cm^3 methanol was added. The reaction mixture was heated and stirred until the dissolution of the ligand. After about 4 days, the crystals formed were filtered-off, washed with methanol and dried in air at room temperature.

The compound with Zn(II) was prepared similarly, except that instead of zinc acetate, zinc chloride was used. When the ligand fully dissolved and the color changed to dark red the reaction mixture was cooled to room temperature. To the cool solution, to adjust the pH, 3 cm^3 of NH_3(aq) was added. A dark red microcrystalline product started to precipitate and was completed in 24 hours.

Analytical data

$[Co_2(\mu\text{-}Hp_2DAP\text{-}2H)_2(\mu\text{-}O_2)]\cdot 4H_2O$ (1). Color: dark red (almost black). Yield: 32.3%. M_r = 1050.44 (found C, 38.9; H, 3.3; N, 24.0, calc. for $C_{34}H_{26}Cl_4Co_2N_{18}O_2\cdot 4H_2O$ C, 38.45; H, 3.20; N, 23.66%). λ_M (S cm^2 mol^{-1}) = 0.50.

$[Ni(Hp_2DAP\text{-}2H)]$ (2). Color: dark brown microcrystalline precipitate. Yield: 80.0%. M_r = 474.97 (found C, 43.0; H, 3.2; N, 26.5, calc. for $C_{17}H_{15}Cl_2N_9Ni$ C, 42.00; H, 2.89; N, 25.63%). λ_M (S cm^2 mol^{-1}) = 0.20.

$[Cu(Hp_2DAP\text{-}2H)]\cdot H_2O$ (3). The reaction mixture was diluted by 5 cm^3 methanol. Color: dark brownish-red microcrystalline precipitate. Yield: 71.5%. M_r = 497.83 (found C, 41.0; H, 3.4; N, 25.3, calc. for $C_{17}H_{15}Cl_2CuN_9.H_2O$ C, 41.78; H, 3.10; N, 25.07%). λ_M (S cm^2 mol^{-1}) = 0.00.

$[Zn(Hp_2DAP\text{-}2H)]\cdot H_2O$ (4). Color: dark red microcrystalline precipitate. Yield: 75.2%. M_r = 499.68 (found C, 40.9; H, 3.4; N, 25.2 calc. for $C_{17}H_{15}Cl_2N_9Zn\cdot H_2O$ C, 41.26; H, 3.11; N, 25.35%). λ_M (S cm^2 mol^{-1}) = 0.20.

Physical measurements

IR data were collected on a Thermo Nicolet Nexus 670 FT-IR spectrometer at room temperature in the range of 4000–400 cm^{-1} with resolution of 4 cm^{-1} using KBr pellets.

Raman spectra were obtained with the LabRAM system (Horiba Jobin-Yvon, Lyon, France) coupled with an external 532 nm Nd-YAG laser source (Sacher Lasertechnik, Marburg, Germany) and an Olympus BX-40 optical microscope (Olympus, Hamburg, Germany). The resolution of the Raman instrument was *ca.* 3 cm^{-1} in the 4000–200 cm^{-1} spectral range and a backscattered geometry was used. For the measurements solid samples were used.

The molar conductivity of freshly prepared 1×10^{-3} mol dm^{-3} solutions of the complexes in *N*,*N*′-dimethylformamide (DMF) was determined at room temperature using a digital conductivity meter (Jenway 4010).

TG/DSC measurements were carried out on a TA Instruments SDT Q600 thermal analyzer with 20 °C min^{-1} heating rate in the range from room temperature to 700 °C and sample mass <3 mg. Carrier gases: nitrogen, air. Gas flow rate: 100 cm^3 min^{-1}. Sample holder/reference: alumina crucible/empty alumina crucible.

Cell lines and cultures

L5178Y parental (PAR) mouse T-cell lymphoma cells (ECACC cat. no. 87111908; U.S. FDA, Silver Spring, MD, USA) were transfected with pHa *MDR1*/A retrovirus as described previously.[2] The ABCB1-expressing cell line (MDR) was selected by culturing the transfected cells with 60 ng cm^{-3} of colchicine (Sigma-Aldrich Chemie GmbH, Steinheim, Germany) to maintain the MDR phenotype. The cells were cultured in McCoy's 5A medium (Sigma)

supplemented with L-glutamine (Sigma) and antibiotics (penicillin/streptomycin solution, Sigma) at 37 °C and in an atmosphere with 5% CO_2.

Assay for antiproliferative and cytotoxic effect

The effects of increasing concentrations of the compounds on cell growth were tested in 96-well flat-bottomed microtiter plates. The compounds were diluted in 100 μL medium then 6×10^3 cells for antiproliferative assay or 2×10^4 cells for cytotoxic assay in 100 μL of medium, were added to each well, with the exception of the medium control wells. The compounds were dissolved in DMSO. The solvent applied in the assays had no effect on cell growth. The culture plates were further incubated at 37 °C for 72 h and 24 h. At the end of the incubation period 20 μL of 3-(4,5-dimethyl-2-thiazolyl)-2,5-diphenyl-2*H*-tetrazoliumbromide (MTT, Sigma-Aldrich Chemie GmbH) solution (from a 5 mg cm^{-3} stock) were added to each well. After incubation at 37 °C for 4 h, 0.10 cm^3 of sodium dodecyl sulfate (SDS, Sigma) solution (10% in 0.01 mol dm^{-3} HCI) were added to each well and the plates further incubated at 37 °C overnight. The cell growth was then determined by measuring the optical density (OD) at 550 nm (ref. 630 nm) with a Multiscan EX ELISA reader (Thermo Labsystems, Cheshire, WA, USA).

Assay for reversal of MDR in tumor cells by flow cytometry

L5178Y parental (PAR) and multidrug resistant (MDR) mouse T-cell lymphoma cells were adjusted to a density of 2×10^6 cells cm^{-3}, resuspended in serum-free McCoy's 5A media and distributed in 0.5 cm^3 aliquots (1×10^6 cells). The cells were incubated in the presence of the ligand and its complexes for 10 min at room temperature. Then, the fluorescent ABCB1 substrate rhodamine 123 (R123, Sigma-Aldrich) was added to each sample at a final concentration of 5.2 μM and the cells were incubated for 20 min at 37 °C in a water bath, washed twice and resuspended in 0.5 cm^3 phosphate-buffered saline (PBS) for analysis. The fluorescence of the cell population was measured with a Partec CyFlow flow cytometer (Partec, Münster, Germany). Verapamil hydrochloride (EGIS Pharmaceuticals PLC, Budapest, Hungary) was used as a positive control in MDR cells at a final concentration of 10 μg cm^{-3}.[13]

Representative flow cytometric experiments with 1×10^4 cells were evaluated for the accumulation of R123.[13] The fluorescence activity ratio (FAR) for L5178Y/PAR and L5178Y/MDR cell lines was calculated using the following equation:

$$\mathrm{FAR} = \frac{\mathrm{MDR_{treated}}/\mathrm{MDR_{control}}}{\mathrm{Parental_{treated}}/\mathrm{Parental_{control}}}$$

The results provided are from a representative flow cytometric experiment in which 10 000 individual cells were evaluated. Partec CyFlow flow cytometer research software was used to analyze the recorded data. The data were first presented as histograms and were converted to FAR units that define fluorescence intensity, standard deviation, and peak channel in the total and in the gated populations.

X-ray crystallography

Single-crystal X-ray diffraction data for **1** were collected at room temperature on an Oxford Diffraction Gemini S diffractometer with Mo-Kα radiation (λ = 0.71073 Å). Data collection, unit cell finding, intensity integration and scaling of the reflections were performed with the CRYSALISPRO software.[14] Empirical absorption correction using spherical harmonics, implemented in the SCALE3 ABSPACK scaling algorithm within CRYSALISPRO was applied. The crystal structure was solved with SHELXT[15] and refined using SHELXL-2014[16] with SHELXLE[17] as the graphical interface.

All non-hydrogen atoms were refined anisotropically. The hydrogen atoms attached to the carbon atoms were placed at geometrically idealized positions with C–H distances fixed to 0.93 and 0.96 Å and their isotropic displacement parameters set equal to 1.2 U_{eq} and 1.5 U_{eq} of the parent sp^2 and sp^3 C atoms, respectively. X-ray diffraction data did not allow unambiguous determination of the H-atoms bonded to crystal water molecules in difference electron density maps.

A summary of the pertinent crystallographic data are given in Table 1. The ORTEP-3 and WINGX software were used for the preparation of the materials for publication.[18]

Computation details

All density functional theory (DFT) calculations were performed using the Jaguar 8.7 program,[19] as implemented in the Schrödinger Material Suite release 2015-1 (Schrödinger, LLC, New York, NY, 2015). DFT calculations for structures containing transition metals were performed using B3LYP[20a–c] exchange–correlation functional

Table 1 Crystallographic data for crystal structure of **1**

Molecular formula	$C_{34}H_{26}Cl_4Co_2N_{18}O_2{\cdot}4H_2O$
Formula weight	1050.45
Color, crystal shape	Dark red, prism
Crystal size (mm^3)	0.52 × 0.13 × 0.04
Temperature (K)	293(2)
Wavelength (Å)	0.71073
Crystal system	Monoclinic
Space group	*C*2/*c*
a (Å)	12.7108(4)
b (Å)	22.8673(5)
c (Å)	14.7326(3)
α (°)	90
β (°)	94.369(2)
γ (°)	90
V ($Å^3$)	4269.76(19)
Z	4
D_{calc} (Mg m^{-3})	1.634
μ (mm^{-1})	1.095
θ range for data collection (°)	3.12–29.07
Reflections collected	16 829
Independent reflections, R_{int}	5072, 0.0275
Completeness to θ = 26.32° (%)	99.9
Data/restraints/parameters	5072/0/291
Goodness-of-fit on F^2	1.053
Final R_1, wR_2 indices ($I > 2\sigma_I$)	0.0375, 0.0934
Final R_1, wR_2 indices (all data)	0.0548, 0.1007
Largest diff. peak & hole (e $Å^{-3}$)	0.402 and −0.241

where $R_1 = \sum||F_o| - |F_c||/\sum|F_o|$; w$R_2 = [\sum(w(F_o^2 - F_c^2)^2)/\sum(wF_o^2)^2]^{1/2}$; GoF $= [\sum(w(F_o^2 - F_c^2)^2)/(n-p)]^{1/2}$, *n* is the number of reflections, and *p* is the number of refined parameters.

with LACV3P+(d,p) basis set, whereas the ligand structure was investigated again using the B3LYP exchange–correlation functional with 6-31+G(d,p) basis set. A C_2 symmetry constraint during geometrical optimization was employed for the binuclear cobalt(III) complex **1**, whereas the other assumed structures were geometrically optimized without symmetry constraints. After successful geometrical optimization, a single point energy calculation was run to obtain additional information on molecular electrostatic potential (MEP) and average local ionization energy (ALIE) surfaces.

Results and discussion

Synthesis of compounds

The bis(3-chloropyridazine-6-hydrazone)-2,6-diacetylpyridine (**Hp_2DAP**) ligand was synthesized according to the procedure described in our previous study[10] but instead of methanol the reactions were carried out in acetonitrile. In the reaction between the hydrazine group of 3-chloro-6-hydrazinopyridazine and the carbonyl groups of 2,6-diacetylpyridine a new Schiff-base was formed with five potential coordinating N atoms (Fig. 1).

Hp_2DAP is not soluble in methanol, but its warm suspension reacts with transition metal ions in the presence of a proton acceptor. Therefore, for the synthesis, the acetate salts of Co(II), Ni(II) and Cu(II) were used. In the case of Zn(II), the salt was zinc(II) chloride and the deprotonation of **Hp_2DAP** to $Hp_2DAP\text{-}2H^{2-}$ was promoted by the addition of ammonia.[21] With Ni(II), Cu(II) and Zn(II), the expected neutral coordination compounds were formed but with cobalt(II) acetate the reaction route was different. In air, during the complex formation, Co(II) was oxidized to Co(III) and water to peroxide and a dimeric coordination compound $[Co_2(\mu\text{-}Hp_2DAP\text{-}2H)_2(\mu\text{-}O_2)]\cdot 4H_2O$ (**1**) with a peroxido bridge between the Co(III) centres was formed. The reaction is highly repeatable and probably occurs by a complex mechanism, yet the yield is rather low, compared to the yields of the other compounds. The molar conductivity data refer to the non-electrolytic character of all four coordination complexes, in accordance with the coordination of the ligand in its doubly deprotonated form.[22]

Crystal and molecular structure of complex 1

Single-crystal X-ray analysis shows that the complex of Co(III) and **Hp_2DAP** ligand (**1**) is a neutral binuclear coordination complex with two symmetrically related halves (Fig. 2 and 3).

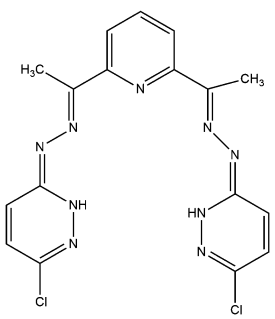

Fig. 1 Structure of **Hp_2DAP**.

The crystallographic asymmetric unit also includes two water molecules of crystallization and therefore the crystal structure can be described by the formula $[Co_2(\mu\text{-}Hp_2DAP\text{-}2H)_2(\mu\text{-}O_2)]\cdot 4H_2O$. **$Hp_2DAP$** contains two arms bonded to the central pyridine ring in the same positions regarding the N1 nitrogen atom. These two arms are denoted as A and B in Fig. 2 and 3 using the suffixes a and b in atomic labels. A and B have equal compositions but very different orientations with regard to the pyridine ring. While arm A is approximately coplanar with the pyridine ring, arm B is considerably displaced from the plane of the central ring (Fig. 2). This structural difference between A and B can be illustrated well by comparison of the N1–C–C6–N2 torsion angles [−1.4(3)° and 71.1(3)° for A and B, respectively]

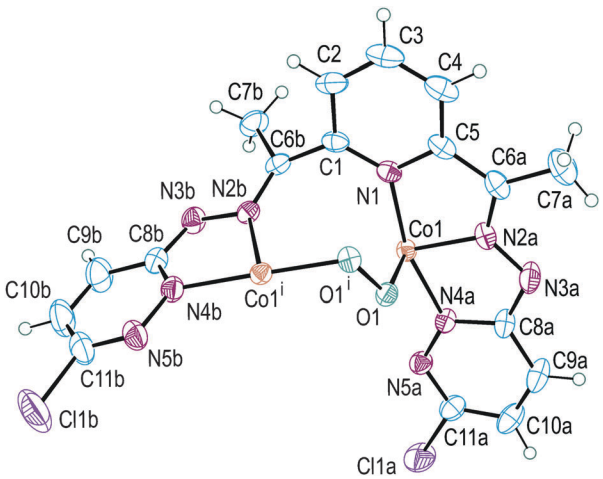

Fig. 2 Asymmetric unit of complex **1** with atom numbering scheme. Crystal water molecules are omitted for clarity. The $Co1^i$ and $O1^i$ atoms [symmetry code: (i) $-x, y, -z + 0.5$] do not belong to the same asymmetric unit. Displacement ellipsoids of non-H atoms are drawn at the 40% probability level.

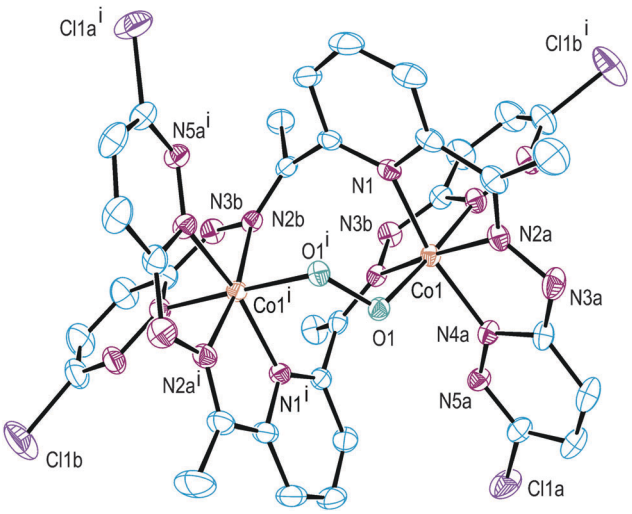

Fig. 3 Binuclear unit of complex **1**. H atoms and water molecules are omitted for clarity. Displacement ellipsoids are drawn at the 30% probability level.

and dihedral angles between pyridine ring and the terminal N4–N5 ring [10.36(15)° for A and 79.29(9)° for B]. All non-H atoms are roughly coplanar in both moieties but the fragment B is somewhat more puckered as is mainly demonstrated in the value of the C6–N2–N3–C8 torsion angles [179.1(2)° and −164.5(2)° for A and B, respectively].

All the abovementioned structural differences between arms A and B can be explained by their different coordination behaviour. Namely, the A moiety is coordinated to the Co atom together with the N1 atom, whereas the B fragment is coordinated to the neighbouring Co1^{i} atom [symmetry code: (i) $-x, y, -z + 0.5$] forming a bridge between the two metal atoms in the binuclear unit (Fig. 2 and 3). The moiety A together with the pyridine nitrogen form two fused five-membered chelate rings that are almost ideally coplanar [dihedral angle between two chelate rings is 2.11(13)°]. The B fragment is coordinated to the metal atom through the same nitrogen atoms, the N2 and N4, as is the case for A. However, the Co–N2 coordination bond for B is almost 0.13 Å longer than the corresponding bond for the A moiety. Such a high difference between the two equal coordination bonds is also surprising because the N2a and N2b atoms are chemically identical and (mutually) situated in a *trans* position regarding the Co1 atom. An explanation could be found in the supposed orientation of the nitrogen's (N2a) lone electron pair regarding the metal atom. Because the N2 atom is sp^2 hybridized it is reasonable to expect that its lone pair lies in the same plane as the C6–N2–N3 fragment. In the case of the A fragment, the Co atom lies perfectly in the C6–N2–N3 plane and consequently the location of the metal atom corresponds very well with the orientation of the nitrogen's lone pair. This enables a relatively strong Co–N2a coordination bond. In the case of fragment B, the Co atom is significantly displaced from the C6–N2–N3 plane [displacement of 0.205(7) Å] and consequently the Co1–N2b bond is significantly weaker and longer than that in fragment A [1.8691(18) Å for A and 1.9945(17) Å for B]. Herein, we can also add the information that the Co–N2a and corresponding Co–N2b are the shortest and the longest coordination bonds, respectively, in the crystal structure of complex **1** (Table 2).

The interesting coordination mode of the **Hp$_2$DAP** ligand in the present structure and the different structural behaviour of the two moieties are directly related to the coordination geometry of the Co(III) atom. The metal atom in **1** is coordinated in a rather distorted octahedral arrangement by the N_5O donor set (Fig. 4). The N2a–Co1–N4a, N1–Co1–N2a and N2b–Co–N4b coordination angles (Table 2) significantly deviate from 90°, whereas the N1–Co1–N4a coordination angle of 162° considerably deviates from an ideal value of 180°. This could be expected due to formation of five-membered chelate rings (influence of two fused chelate rings in the case of the N1–Co1–N4a angle). However, some coordination planes are also significantly deformed. Thus, the Co1, N1, N2a, N4a are nearly coplanar (root-mean-square deviation of fitted atoms is only 0.012 Å), whereas the N2b^{i} atom, which lies in the same coordination plane, is displaced from the Co1–N1a–N2a–N4a mean plane by 0.286(3) Å. The two equivalent angles, C1–N1–Co1 and C5–N1–Co1, should have very similar values but in the crystal structure of **1** these bond angles are very different [130.19(16)° and 111.15(15)°, respectively]. This means that the Co1–N1 coordination bond does not coincide well with the direction of the lone pair of the N1 atom.

Table 2 Selected bond distances (Å) and coordination angles (°) in the crystal structure of complex **1**. Symmetry code: (i) $-x, y, -z + 0.5$

Bond length	Å	Bond angle	°
Co1–N2a	1.8691(18)	N2a–Co1–N4a	80.52(8)
Co1–O1	1.8843(14)	O1–Co1–N4a	88.49(7)
Co1–N4a	1.9187(18)	N2a–Co1–N4b^{i}	93.04(8)
Co1–N4b^{i}	1.9399(19)	O1–Co1–N4b^{i}	176.30(7)
Co1–N1	1.9685(18)	N4a–Co1–N4b^{i}	94.73(8)
Co1–N2b^{i}	1.9945(17)	N2a–Co1–N1	82.17(8)
O1–O1^{i}	1.416(3)	O1–Co1–N1	89.66(7)
N1–C1	1.339(3)	N4a–Co1–N1	162.62(8)
N1–C5	1.369(3)	N4b^{i}–Co1–N1	87.81(8)
N2a–C6	1.290(3)	N2a–Co1–N2b^{i}	170.29(8)
N2a–N3a	1.357(3)	O1–Co1–N2b^{i}	97.88(7)
N3a–C8a	1.331(3)	N4a–Co1–N2b^{i}	93.06(7)
N4a–N5a	1.343(3)	N4b^{i}–Co1–N2b^{i}	80.16(8)
N4a–C8a	1.362(3)	N1–Co1–N2b^{i}	104.32(7)
N2b–C6b	1.296(3)		
N2b–N3b	1.391(3)		
N3b–C8b	1.336(3)		
N4b–C8b	1.350(3)		
N4b–N5b	1.350(3)		
C1–C6b	1.479(3)		
C5–C6a	1.446(4)		

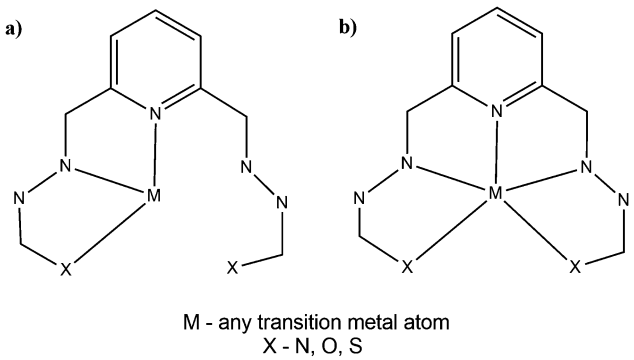

Fig. 4 (a) Structural fragment used in the CSD search. (M is any transition metal, X is an N, O or S atom). (b) The most frequent coordination mode found in 116 crystal structures, which contain the fragment is shown in (a). All donor atoms are roughly coplanar with the metal atom.

The abovementioned analysis demonstrates very interesting structural characteristics and exceptional flexibility of the **Hp$_2$DAP** ligand. In the Cambridge Structural Database (CSD, Version 5.34, May 2013),[23] we found 150 crystal structures of transition metal complexes with very similar ligands to complex **1** (Fig. 4a). The **Hp$_2$DAP** derivatives are mainly coordinated as pentadentate ligands (116 crystal structures) with the coordination mode illustrated in Fig. 4b. Binuclear complexes are not rare but complex **1** is the only example, which contains a peroxido bridge between two metal centres (O1–O1^{i} in Fig. 3). In the CSD, there are 26 crystal structures that contain the fragment shown in Fig. 4a and the Co metal atom. All Co(II) complexes have coordination mode, as shown in Fig. 4b, and only one of them is

binuclear[24] but with the same coordination mode. There are additional two binuclear complexes,[23,25] both with Co(III) metal centres and have, as well as Co(II) binuclear complexes, different coordination modes than that presented in **1**. Recently, we have reported the crystal structure of a Co(III) complex[10] with the same donor set and very similar ligand to **Hp_2DAP** as in **1**, but in that case the complex molecule crystallized as discrete mononuclear units. A comparison of structural data for all 150 structures extracted from CSD also showed that complex **1**, along with some Ni complexes[26a–d] form one of the shortest M–N2 bonds in transition metal complexes with DAP derivatives. One can conclude that the presented binuclear Co(III) complex **1** has some interesting structural characteristics and a coordination mode, which is observed for the first time in Co complexes with similar ligands.

IR spectral data

In the ligand, the characteristic νNH bands appear at *ca.* 3400 cm^{-1}. Due to the deprotonation of the two N atoms of the two pyridazine rings **Hp_2DAP** coordinates through deprotonated N atoms. The intensity of the skeleton vibration bands in the regions of ~1400–1500 cm^{-1} and ~1100–1200 cm^{-1} increases and in the spectra of **2**, **3** and **4** the bands are overlapped compared to those in the ligand. The characteristic vibrations for the compounds are listed in Table 3.

As a consequence of complex formation, the change in the mutual orientations of the methyl groups results in additional νCH vibrations appearing in the spectra of the complexes, especially in that of **1**. In the spectrum of **1**, further band splitting is observed related to its dimeric structure. These differences prove the coordination of the ligand through its N atoms and refer to the structural differences between **1** and the other three coordination complexes. The characteristic vibration around 860 cm^{-1} in **1** for the –O–O– group is active in the Raman due to its symmetry. The ligand and coordination complexes **1** and **4** were also characterized by Raman spectra (Fig. 5). The other two compounds **2** and **3** were not suitable for Raman measurements. For the detection of the peroxido bridge, the most interesting region is in the range from ~900 cm^{-1} to ~400 cm^{-1}. The Raman band of μ-O_2 appears at lower energy than the band of the side-on peroxido groups,[27] which usually appears somewhat above 850 cm^{-1}.[28a,b] In the spectrum of **1** (Fig. 5), the most intensive sharp peak at 691 cm^{-1} and the next one at 621 cm^{-1} can be assigned as peroxide vibrations, whereas the other two peaks presumably belong to Co–O vibrations. Comparing all three spectra, it is obvious that compound **4** gives similar bands as the ligand and does not contain a peroxido group.

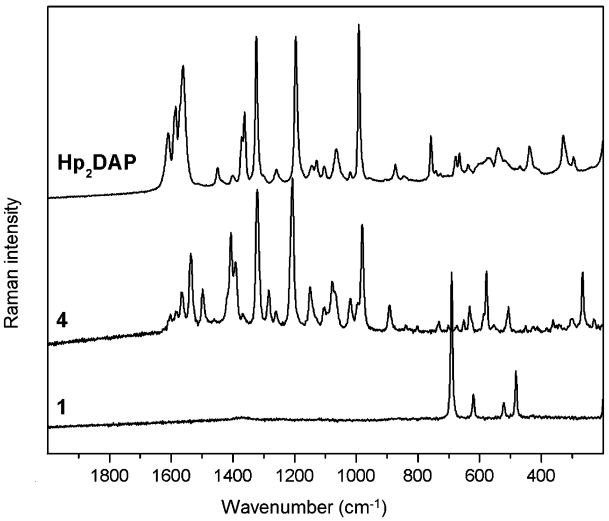

Fig. 5 The Raman spectra of **Hp_2DAP**, **1** and **4**.

Results of DFT calculations: MEP and ALIE surfaces

To obtain an insight into the reactive properties of the structures computationally investigated in this study we shall refer to the MEP and ALIE surfaces.

MEP surfaces present a very useful descriptor to determine potential sites prone to electrophilic attack and nucleophilic reactions.[29a–c] This descriptor is important as it is related to the charge distribution of the investigated molecule. Employing MEP, one is able to determine how molecules interact with other molecules or radicals. The MEP (hereafter indicated as $V(r)$) is given as follows:

$$V(\vec{r}) = \sum \frac{Z_A}{|R_A - \vec{r}|} - \int \frac{\rho(\vec{r}')}{|\vec{r}' - \vec{r}|} d\vec{r} \quad (1)$$

where the summation runs over all nuclei A with charge Z_A and coordinate R_A, whereas $\rho(r')$ is the electron density of the molecule. $V(r)$ represents the potential exerted at the coordinate r by the nuclei and the electrons. The sign of $V(r)$ at any point depends on whether the effects of the nuclei or the electrons are dominant.[30a,b] The last equation is valid when polarization and nuclear rearrangement effects due to the presence of a unit test charge at the distance r are neglected.

Another very useful indicator of molecule's reactivity is its ALIE surface. ALIE is defined as a sum of orbital energies

Table 3 Characteristic FTIR bands of the compounds

Vibration	**Hp_2DAP** [cm^{-1}]	**1** [cm^{-1}]	**2** [cm^{-1}]	**3** [cm^{-1}]	**4** [cm^{-1}]
νC–H	3430–2850	3410–2840	3430–2850	3435–2850	3425–2845
νring	1590–1500	1590–1500	1580–1495	1580–1495	1585–1495
νC═N	1450–1400	1465–1395	1465–1385	1460–1390	1450–1395
νC_{Ar}–N	1370	1335–1285	1325–1285	1330–1265	1325–1285
δring, δC═N, νC═N, δCH_3	1130–1020	1160–1040	1165–1025	1145–1025	1150–1025
τN–H	875–805	—	—	—	—
νC–Cl	730–675	750–645	730–635	730–635	730–630

weighted by the orbital densities[31a,b] and this approach represents an energetic measure of how easy or difficult is it to remove electrons from certain areas of the molecule. It was demonstrated by Sjoberg[31] and Murray[32] that the ALIE $I(r)$ plotted on a molecular surface is a fine strategy to understand chemical reactivity in aromatic systems.[29b,32] $I(r)$ is defined in the following manner:

$$I(r) = \sum_i \frac{\rho_i(\vec{r})|\varepsilon_i|}{\rho(\vec{r})} \quad (2)$$

where $\rho_i(\vec{r})$ is the electronic density of the i-th molecular orbital at the point $\vec{r}$, ε_i is the orbital energy, while the $\rho(\vec{r})$ is the total electronic density function. Using Koopman's theorem, $I(r)$ can be interpreted as the average energy needed to ionize an electron at any particular point $\vec{r}$ in the space of a molecule. Therefore, the locations in the molecule wherein the ALIE has the lowest values represent areas of the least tightly bound electrons and sites to be most reactive towards electrophiles.[29b,30b] The equilibrium geometries and the MEP and ALIE surfaces for **1** and **Hp_2DAP** are presented in Fig. 6. It should be noted that both MEP and ALIE surfaces were mapped on the electron density surface.

The MEP surface of **Hp_2DAP** indicates that the lowest electrostatic potential is located (to small extent) in the near vicinity of the central nitrogen (N2) atom. However, the ALIE surface of the ligand identifies the locations of nitrogen atoms as centres suitable for electrophilic attack. Electron density marked by a red color is located in a significant amount precisely on these atoms.

In **1** both MEP and ALIE surfaces indicate that from the aspect of electrophilic attacks, the important reaction sites could be the central part of complex at the location wherein the oxygen atoms are placed. According to the MEP surface, the oxygen atoms should be considered as the most important reaction sites, whereas the ALIE surface indicates that nitrogen atoms also represent potential reaction sites, because at these locations, the electrons are also less tightly bound.

The proposed geometries for compounds **2–4** are depicted in Fig. 7. The lowest values of MEP for the proposed structures are practically the same for the coordination compounds **2–4**. On the other hand, the maximum value of MEP for the structure containing the Zn(II) atom (**4**, Fig. 7) is two times higher than that for **2** and **3** (Fig. 7), whereas the latter two have almost identical values for maximum values of the MEP. Concerning the charge distribution according to the MEP surfaces, it can be observed that in all cases, the nitrogen atoms of the ligand, which are not coordinated are recognized as significant reaction sites, as at these locations MEP has the lowest values (indicated by the red color in Fig. 7). The lowest values of MEP can be found in the pocket around the central atoms in **2–4**. The highest value of MEP among all three mononuclear complexes is found in **4** and is located practically on the zinc atom (Fig. 7).

ALIE surfaces also indicate the reactive significance of nitrogen atoms and the neighbouring metal centres, as at these locations the electrons are the least tightly bound (indicated by the red color in Fig. 7), which is in agreement with the MEP surfaces. In the case of **2**, significant red color is located precisely at the nickel atom. Moreover, the yellow-to-red color of ALIE surfaces located in the

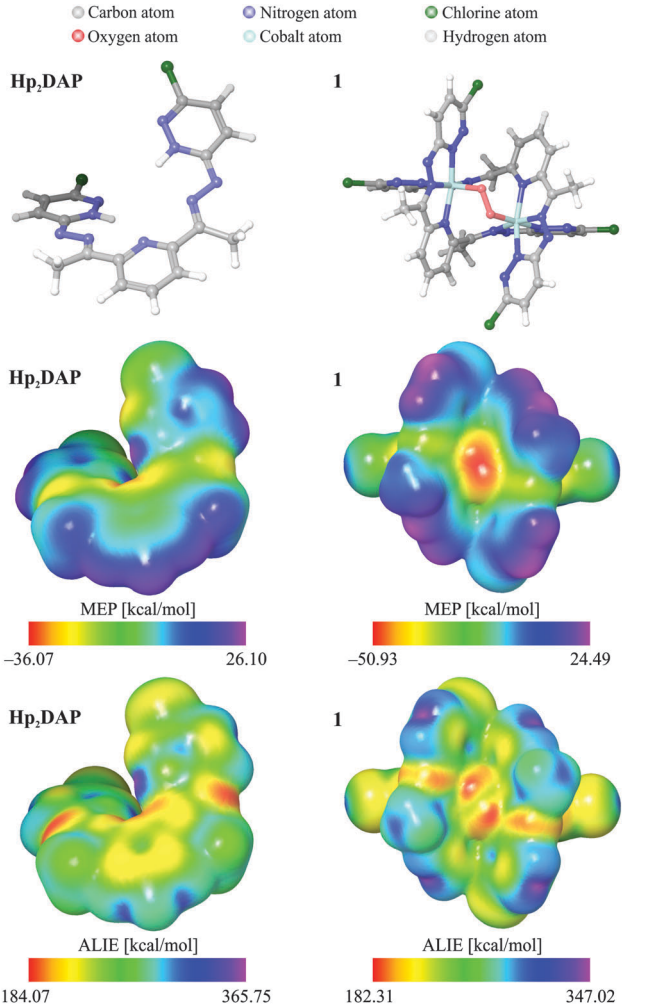

Fig. 6 Geometries of optimized **Hp_2DAP** and **1** and the corresponding MEP and ALIE surfaces.

near vicinity of other nitrogen atoms for the calculated structures **2–4** identifies these sites as interesting ones from the aspect of electrophilic attacks.

In Table 4, the calculated dipole moment, μ, the polar surface area (PSA) and the total surface area (TSA) are presented along with the molecular lipophilicity.[33] The measure of the molecular lipophilicity is the log P (the logarithm of the 1-octanol/water partition coefficient) marked as $A\log P$.

The influence of DMSO solvent on the geometries of the complexes has also been investigated through DFT calculations (for the details, see ESI†). It was found that although the solvent significantly rotated the pyridazine moiety around the N–N bond, complexes **2** and **3** preserved their square-planar coordination geometry. For **4**, geometrical optimizations with the solvent resulted in unreasonable geometries. This phenomenon is most probably due to the proposed unfavorable square-planar geometry around the zinc centre.

Thermal data for Hp_2DAP and 1–4

The thermal stability of new compounds is sometimes crucial for their potential application.[34] In addition, thermal data may

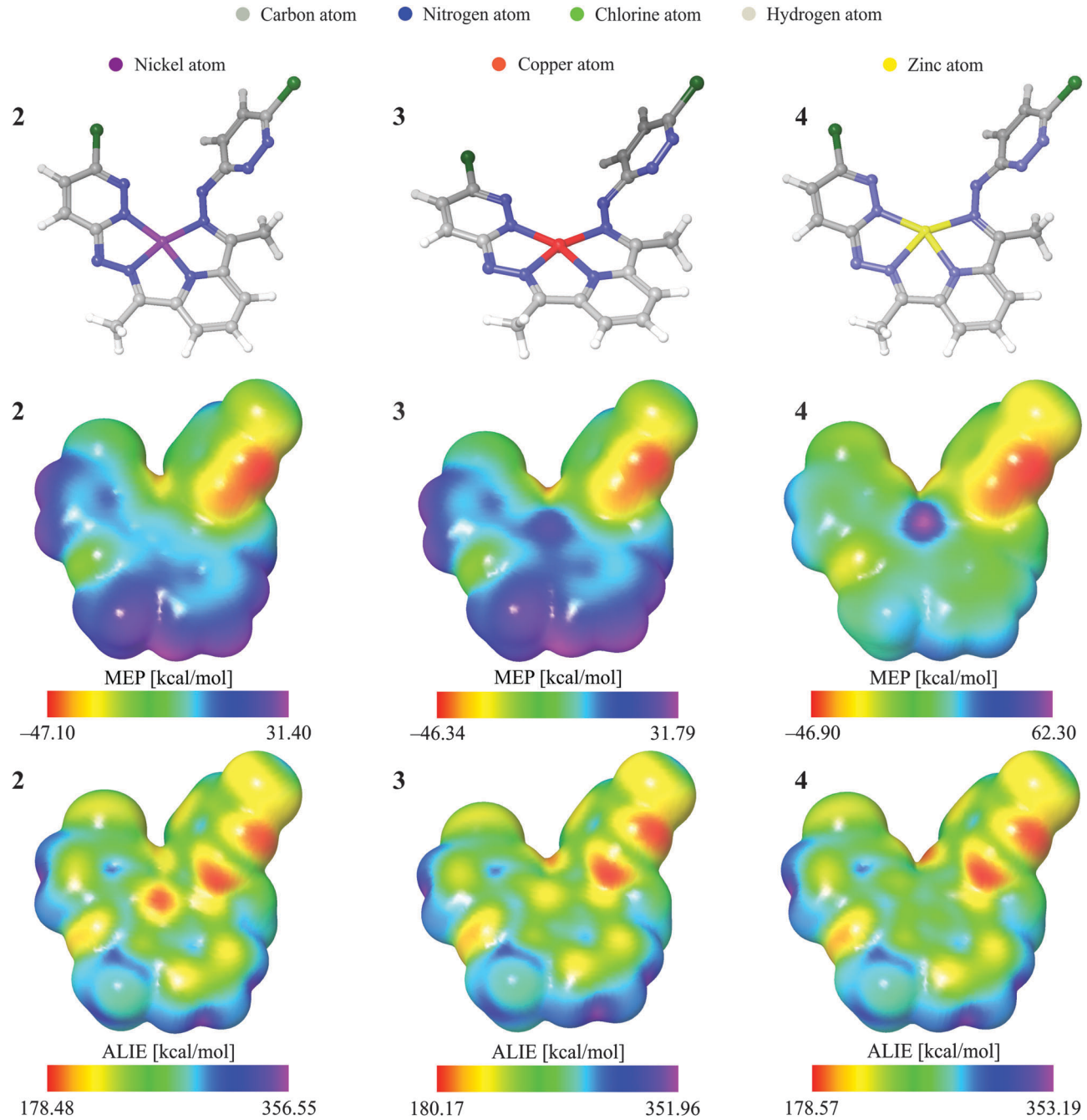

Fig. 7 Geometries of the proposed structures for **2**, **3** and **4** and the corresponding MEP and ALIE surfaces.

Table 4 Calculated dipole moment, polar surface area, total surface area and *A* log *P* of **Hp_2DAP** and **1–4**

Sample code	μ [D]	PSA [Å^2]	TSA [Å^2]	*A* log *P*
Hp_2DAP	2.23	119.69	664.73	3.22
1	0.24	147.10	924.91	3.70
2	8.56	76.00	617.12	0.33
3	8.56	76.00	631.31	0.33
4	8.84	76.00	642.65	0.33

be valuable in detecting even small structural differences.[35] As only the molecular structure of **1** was determined by X-ray structure analysis, the compounds were characterized also by means of TG-DSC measurements and their thermal decomposition patterns were compared.

The **Hp_2DAP** ligand is stable up to 200 °C and its thermal decomposition does not depend on the atmosphere up to 400 °C. A sharp endothermic effect around 300 °C refers to the decomposition accompanied by melting of the ligand, which was also observed visually.

The heat effects accompanying the decomposition reactions in complex compounds in a nitrogen atmosphere are presented by the corresponding DSC curves in Fig. 8. The structural

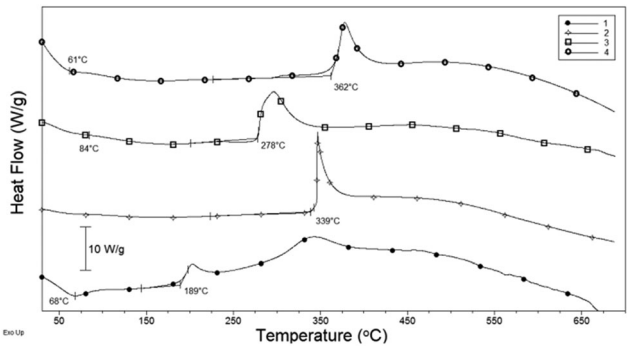

Fig. 8 DSC curves for coordination compounds.

preferences of the central atoms can be clearly observed in the corresponding DSC curves. In compound **1**, with a dimeric structure and a peroxido bridge, the most favorable octahedral surround is established around cobalt(III). Moreover, both deprotonated $Hp_2DAP\text{-}2H^{2-}$ are coordinated to both Co(III) centres as bridges. This arrangement results in relatively low repulsions between the ligands. The peroxido group is heat sensitive; therefore, the decomposition of anhydrous **1** starts with exothermic processes due to oxidation reactions with the peroxido group. These reactions are missing in compounds **2–4** (Fig. 8). The strong electrostatic interactions (supported by the high value of MEP around the Zn metal centre) result in the significantly higher thermal stability of **4**. A similar effect was observed in the case of a Zn(II) complex with bis(phthalazine-1-hydrazone)-2,6-diacetylpyridine.[10]

Cytotoxic activity evaluation

The biological activity of **Hp_2DAP** and its coordination compounds with Co(III) **1**, Ni(II) **2**, Cu(II) **3** and Zn(II) **4** was studied on antiproliferative effects, cytotoxic effects and inhibitory effect of the ABC transporter *P*-glycoprotein encoded by human *MDR1* gene on tumor cells. This transporter protein is responsible for the pumping out, *i.e.* the removal of anticancer drugs from the tumor cells and as a consequence the cell will overgrow despite the chemotherapy. For these *in vitro* experiments, the human *MDR1* gene transfected mouse lymphoma cells were applied. In the flow cytometry, the effects of the compounds were studied on the drug accumulation in MDR cells in short (20 minutes) experiments in flow cytometry. The rhodamine 123 accumulation in *MDR1* gene transfected cells was reduced in the presence of **Hp_2DAP**, **1** and, to some extent, **4**; however, complexes **2** and **3** were ineffective in the applied 8 μg cm^{-3} concentration when the results were compared to the positive control, Verapamil, applied in a concentration of 10 μg cm^{-3}. The results are shown in Table 5.

Apparently, there is some structure–activity relationship between the chemical structures of the hydrazine derivative and its coordination complexes and the inhibition of PGP-170 (*P*-glycoprotein, PGP, ABCB1, *MDR1*, $M_r \sim 170$) mediated multidrug resistance of cancer cells. The cytotoxic effects of all the compounds measured on the parent drug sensitive PAR and drug resistant MDR cells showed no difference between the

Table 5 Reversal of multidrug resistance of human *MDR1* gene transfected mouse lymphoma cells in the presence of the **Hp_2DAP** ligand and its complexes

Sample code	Conc. (μg cm^{-3})	FSC	SSC	FL-1	FAR
Verapamil	10	2525	1279	5.86	7.38
Hp_2DAP	2	2524	1346	6.78	8.53
1	2	2476	1245	8.49	10.69
2	2	2463	1248	1.65	2.08
3	2	2527	1248	1.50	1.89
4	2	2499	1302	3.98	5.01

where FSC stands for forward scatter count, SSC for side scatter count, FL-1 for fluorescence of the cell population and FAR is the fluorescence activity ratio.

sensitivity of the two cancer cell lines, meaning they are not substrates for the *MDR1* gene-coded drug efflux.

Significant differences were detected for the compounds regarding the antiproliferative effects and the drug accumulation in MDR cells. The evidence shows that the cobalt(III) compound **1** was the most effective inhibitor of the ABC transporter PGP drug efflux pump that is responsible for extruding the anticancer drugs from cancer cells in *in vitro* studies. The zinc(II) complex **4** showed about half the effect when compared to **1**, whereas the compounds with Ni(II) **2** and Cu(II) **3** were practically inactive. Interestingly, the antiproliferative effects of the ligand were only slightly lower than those of **1** but significantly higher than those of **4**. The same trend was observed in the rhodamine 123 accumulation. The accumulation in *MDR1* gene transfected cells was reduced in the order of **4** < **Hp_2DAP** < **1** in the presence of the compounds.

It is known that the coordination of the metal affects both the toxicity and the cell penetration of the compounds. Clède[36] found a straightforward relationship between the lipophilicity, cytotoxicity and cellular uptake with the length of the side chain of bio-imaging rhenium triscarbonyl complexes: the increased lipophilicity increased the penetration, which increased the overall toxicity. However, with coordination, the overall charge distribution and the geometry of the molecules also changed. Therefore, metal chelates of Schiff bases may act as PGP inhibitors.[37] The size of the molecules might also be crucial[38] to their bioavailability. On the other hand, drug resistance is caused by different mechanisms and at the different stages of the action. One of the reaction mechanisms is mediated by PGP efflux pump.[39]

Taking into account all these effects and the calculated MEP and ALIE indicators as measures of the molecule's reactivity, it is obvious that the specific symmetry, the relatively high reactive surface and compact structure of complex **1** enhances its biological accessibility. In addition, the most reactive part of the molecule is related to the peroxide bridge that may be a source for singlet $^1O_2$ generation. Reactive oxygen species (ROS) play important roles in cancer cell functions[40] but their role is not yet fully explored.

In **Hp_2DAP**, the charge distribution is more consistent, without the emphasized reaction centres, in comparison with the complexes. In addition, the free ligand is more flexible than its bonded form in the complexes. Just the opposite is true for the complex of zinc **4** wherein the maximum electrostatic potential is located practically at the metal centre in the inner part of the molecule.

The experimentally determined activities correlate well with the calculated dipole moment, the polar surface area (PSA), the total surface area (TSA), and molecular lipophilicity $A\log P$ values (see Table 4). The dipole moment of **1** is by far the lowest (0.24 D) among the compounds. This complex has the highest PSA (147 Å^2) and TSA (925 Å^2) and accordingly, the highest lipophilicity ($A\log P = 3.70$). These parameters show a similar trend in **Hp$_2$DAP**, which, however, has a significantly higher dipole moment (2.23 D), with also relatively high PSA and TSA (120 Å^2 and 665 Å^2, respectively). Its lipophilicity is therefore lower ($A\log P$ = 3.22), but still significantly higher than those for the corresponding complexes **2–4**, which all have very high, but similar dipole moment (>8 D) and small PSA values (76 Å^2). Their total surface areas are comparable with that of the ligand (<650 Å^2). Among them, the highest TSA belongs to the zinc complex **4**.

Conclusions

A new potentially pentadentate nitrogen donor Schiff base ligand, bis(3-chloropyridazine-6-hydrazon)-2,6-diacetylpyridine, **Hp$_2$DAP**, was synthesized by the reaction of 3-chloro-6-hydrazinopyridazine (Hp) and 2,6-diacetylpyridine (DAP). Its coordination compounds were obtained in methanolic suspension of the ligand with Co(II), Ni(II) and Cu(II) acetate solutions, whereas with zinc(II) the reaction was carried out using $ZnCl_2$ and ammonia. The presence of base (acetate ion or ammonia) promoted the double deprotonation of the ligand and neutral complexes were formed. In the case of compounds **2–4**, **Hp$_2$DAP** acted as a tetradentate ligand giving mononuclear complexes with square-planar arrangements around the metal centres. By contrast, with cobalt(II) acetate a binuclear octahedral Co(III) complex **1** was obtained. The Co(III) centres were additionally linked by a peroxide bridge, which was observed in Co(III) complexes for the first time with this type of ligand. A comparison of M–N bond lengths from the CSD showed that the Co(III)–N2 bond was one of the shortest ones in transition metal complexes with DAP derivatives.

The DFT calculations referred to nitrogen atoms of the ligand as suitable centres for electrophilic attacks. In **1**, the peroxido bridge was revealed to be the best site for electrophilic reactions along with the nitrogen atoms of the ligand, which is also true for compounds **2–4**. In **4**, the highest value of MEP is located practically on the zinc atom, in accordance with its coordination preferences, namely, the distorted square-planar geometry is suitable for Ni(II) **2** and Cu(II) **3** but not for Zn(II) **4**.

The cytotoxicity of the compounds was low and in the same range as the reference standard, Verapamil, known also as a calcium channel blocker. The structure–activity relationship between the chemical structures of the compounds and the inhibition of PGP mediated multidrug resistance of cancer cells is not easily recognized. Complexes **1** and **4** along with the ligand **Hp$_2$DAP** exhibited increased inhibitory effect on ABC transporter PGP drug efflux pump in the order of **4** < **Hp$_2$DAP** < **1**, whereas complexes **2** and **3** were almost ineffective in the inhibition of multidrug resistance of cancer cells. The rhodamine 123 accumulation in human *MDR1* gene transfected tumor cells was increased in the same order. Complexes **2** and **3** showed no activity in the flow cytometric studies. This unusual order of activity of the compounds can be related to their physico-chemical and structural properties in accordance with the values of the calculated MEP and ALIE surfaces.

Acknowledgements

The authors thank to the Ministry of Education, Science and Technological Development of the Republic of Serbia for financial support (continuation of the Projects No. ON172014, OI171039, TR34019) and the Secretariat for Science and Technological Development (Autonomous Province of Vojvodina, Republic of Serbia). The authors would like to thank MSc Tamás Firkala for measuring the Raman spectra (Budapest University of Technology, Department of Inorganic and Analytical Chemistry). Moreover, the authors thank I. Ocsovszky (University of Szeged, Department of Biochemistry) and Á. Csonka (University of Szeged, Department of Medical Microbiology and Immunobiology) for the anti-proliferative activity measurements and cytotoxicity tests. Computational part of this study has been performed thanks to the support received from Schrödinger, Inc.

References

1 (*a*) L. A. Torre, F. Bray, R. L. Siegel, J. Ferlay, J. Lortet-Tieulent and A. Jemal, Global cancer statistics, *Ca-Cancer J. Clin.*, 2015, **65**, 87; (*b*) Cancer Facts and Figures, 2016, http://www.cancer.org/acs/.

2 M. M. Gottesman and I. Pastan, *Annu. Rev. Biochem.*, 1993, **62**, 385.

3 (*a*) A. O. Surov, A. P. Voronin, A. A. Simagina, A. V. Churakov, S. Y. Skachilovac and G. L. Perlovich, *New J. Chem.*, 2015, **39**, 8614; (*b*) V. Y. Sosnovskikh, B. I. Usachev and I. I. Vorontsov, *J. Org. Chem.*, 2002, **67**, 6738; (*c*) J. Svete, *J. Heterocycl. Chem.*, 2005, **42**, 361; (*d*) V. Dal Piaz, M. P. Giovannoni, C. Castellana, J. M. Palacios, J. Beleta, T. Domenech and V. Segarra, *J. Med. Chem.*, 1997, **40**, 1417.

4 (*a*) V. Dal Piaz, C. Vergelli, M. P. Giovannoni, M. A. Scheideler, G. Petrone and P. Zaratin, *Il Farmaco*, 2003, **58**, 1063; (*b*) M. P. Giovannoni, C. Vergelli, C. Ghelardini, N. Galeotti, A. Bartolini and V. Dal Piaz, *J. Med. Chem.*, 2003, **46**, 1055.

5 (*a*) M. Campos-Toimil, I. Estévez, E. Raviña and F. Orallo, *Gen. Pharmacol.*, 1998, **30**, 201; (*b*) F. Orallo, *Br. J. Pharmacol.*, 1997, **121**, 1627.

6 (*a*) L. Veronese, E. Q. Procopio, F. De Rossi, T. M. Brown, P. Mercandelli, P. Mussini, G. D'Alfonso and M. Panigati, *New J. Chem.*, 2016, **40**, 2910; (*b*) V. Vrdoljak, J. Pisk, D. Agustin, P. Novak, J. Parlov Vuković and D. Matković-Čalogović, *New J. Chem.*, 2014, **38**, 6176; (*c*) R. B. Viana, A. R. de Souza, B. S. Lima-Neto and A. B. F. da Silva, *Polyhedron*, 2014, **81**, 661; (*d*) B. Warżajtis, B. Đ. Glišić, N. S. Radulović, U. Rychlewska and M. I. Đuran, *Polyhedron*,

2014, **79**, 221; (*e*) S. Rajković, U. Rychlewska, B. Warćzajtis, D. P. Ašanin, D. M. Živković and M. I. Đuran, *Polyhedron*, 2014, **67**, 279.

7 (*a*) U. M. Rafi, D. Mahendiran, A. K. Haleel, R. P. Nankar, M. Doble and A. K. Rahiman, *New J. Chem.*, 2016, **40**, 2451; (*b*) K. R. Grünwald, M. Volpe, P. Cias, G. Gescheidt and N. C. Mösch-Zanetti, *Inorg. Chem.*, 2011, **50**, 7478.

8 (*a*) W. A. Wani, U. Baig, S. Shreaz, R. A. Shiekh, P. F. Iqbal, E. Jameel, A. Ahmad, S. H. Mohd-Setapar, M. Mushtaqueh and L. T. Hun, *New J. Chem.*, 2016, **40**, 1063; (*b*) K. Das, U. Panda, A. Datta, S. Roy, S. Mondal, C. Massera, T. Askun, P. Celikboyun, E. Garribba, C. Sinha, K. Anand, T. Akitsug and K. Kobayashi, *New J. Chem.*, 2015, **39**, 7309; (*c*) J. Cao, J.-C. Liu, W.-T. Deng and N.-Z. Jin, *CrystEngComm*, 2013, **15**, 6359.

9 (*a*) N. Charef, F. Sebti, L. Arrar, M. Djarmouni, N. Boussouali, A. Baghiani, S. Khennouf, A. Ourari, M. A. Al Damen, M. S. Mubarak and D. G. Peters, *Polyhedron*, 2015, **85**, 450; (*b*) M. L. Low, G. Paulus, P. Dorlet, R. Guillot, R. Rosli, N. Delsuc, K. A. Crouse and C. Policar, *BioMetals*, 2015, **28**, 553.

10 B. Holló, J. Magyari, V. Živkovic-Radovanović, G. Vučković, Z. D. Tomić, I. M. Szilágyi, G. Pokol and K. Mészáros Szécsényi, Synthesis, characterisation and antimicrobial activity of bis(phthalazine-1-hydrazone)-2,6-diacetylpyridine and its complexes with Co^{III}, Ni^{II}, Cu^{II} and Zn^{II}, *Polyhedron*, 2014, **80**, 142.

11 A. Hordyjewska, Ł. Popiołek and J. Kocot, *BioMetals*, 2014, **27**, 611.

12 (*a*) F. K. Keter and J. Darkwa, *BioMetals*, 2012, **25**, 9–21; (*b*) P. Szymański, T. Frczek, M. Markowicz and E. Mikiciuk-Olasik, *BioMetals*, 2012, **25**, 1089.

13 D. Szabó, H. Keyzer, H. E. Kaizer and J. Molnár, *Anticancer Res.*, 2000, **20**, 4261.

14 *CrysAlisPro Software system*, Agilent Technologies UK Ltd, Oxford, 2014.

15 G. M. Sheldrick, *Acta Crystallogr., Sect. A: Found. Adv.*, 2015, **71**, 3.

16 G. M. Sheldrick, *Acta Crystallogr., Sect. C: Struct. Chem.*, 2015, **71**, 3.

17 C. B. Hübschle, G. M. Sheldrick and B. Dittrich, *J. Appl. Crystallogr.*, 2011, **44**, 1281.

18 L. J. Farrugia, *J. Appl. Crystallogr.*, 2012, **45**, 849.

19 A. D. Bochevarov, F. Harder, T. F. Hughes, J. R. Greenwood, D. A. Braden, D. M. Philipp, D. Rinaldo, M. D. Halls, J. Zhang and R. A. Friesner, *Int. J. Quantum Chem.*, 2013, **113**, 2110.

20 (*a*) A. D. Becke, *Phys. Rev. A: At., Mol., Opt. Phys.*, 1988, **38**, 3098; (*b*) A. D. Becke, *J. Chem. Phys.*, 1993, **98**, 5648; (*c*) C. Lee, W. Yang and R. G. Parr, *Phys. Rev. B: Condens. Matter Mater. Phys.*, 1988, **37**, 785.

21 B. Holló, Z. D. Tomić, P. Pogány, A. Kovács, V. M. Leovac and K. Mészáros Szécsényi, *Polyhedron*, 2009, **28**, 3881.

22 W. J. Geary, *Coord. Chem. Rev.*, 1971, **7**, 81.

23 F. H. Allen, *Acta Crystallogr., Sect. B: Struct. Sci.*, 2002, **58**, 380.

24 A. Panja, C. Campana, C. Leavitt, M. J. Van Stipdonk and D. M. Eichhorn, *Inorg. Chim. Acta*, 2009, **362**, 1348.

25 A. Panja and D. M. Eichhorn, *J. Coord. Chem.*, 2009, **62**, 2600.

26 (*a*) V. M. Leovac, G. A. Bogdanović, V. I. Češljević and V. Divjaković, *Acta Crystallogr., Sect. C: Struct. Crystallogr. Cryst. Chem.*, 2000, **56**, 936; (*b*) N. C. Kasuga, K. Sekino, C. Koumo, N. Shimada, M. Ishikawa and K. Nomiya, *J. Inorg. Biochem.*, 2001, **84**, 55; (*c*) C. A. Brown, W. Kaminsky, K. A. Claborn, K. I. Goldberg and D. X. West, *J. Braz. Chem. Soc.*, 2002, **13**, 10; (*d*) J. I. Gradinaru, S. T. Malinovskii, M. A. Popovici and M. Gdaniec, *Crystallogr. Rep.*, 2005, **50**, 217.

27 L. Q. Hatcher and K. D. Karlin, Ligand Influences in Copper-Dioxygen Complex-Formation and Substrate Oxidations, in *Advances in Inorganic Chemistry, Homogeneous Biomimetic Oxidation Catalysis*, ed. R. van Eldik and J. Reedijk, 2006, Academic Press, vol. 58, pp. 136–155.

28 (*a*) L. Krivosudský, P. Schwendt, R. Gyepes and J. Šimunek, *Inorg. Chem. Commun.*, 2015, **56**, 105; (*b*) D. I. Kochubey, P. V. Berdnikova, Z. P. Pai, Y. A. Chesalov, V. V. Kanazhevskiy and T. B. Khlebnikova, *J. Mol. Catal. A: Chem.*, 2013, **366**, 341.

29 (*a*) S. Armaković, S. J. Armaković, J. P. Šetrajčić and I. J. Šetrajčić, *J. Mol. Model.*, 2012, **18**, 4491; (*b*) S. Armaković, S. J. Armaković, J. P. Šetrajčić and I. J. Šetrajčić, *Chem. Phys. Lett.*, 2013, **578**, 156; (*c*) R. S. H. Sebastian Sr, M. I. Attia, M. S. Almutairi, A. A. El-Emam, C. Y. Panicker and C. Van Alsenoy, *Spectrochim. Acta, Part A*, 2014, **132**, 295.

30 (*a*) E. Kose, A. Atac, M. Karabacak, C. Karaca, M. Eskici and A. Karanfil, *Spectrochim. Acta, Part A*, 2012, **97**, 435; (*b*) M. Chen, U. V. Waghmare, C. M. Friend and E. Kaxiras, *J. Chem. Phys.*, 1998, **109**, 6854.

31 (*a*) P. Sjoberg, J. S. Murray, T. Brinck and P. Politzer, *Can. J. Chem.*, 1990, **68**, 1440; (*b*) P. Politzer, F. Abu-Awwad and J. S. Murray, *Int. J. Quantum Chem.*, 1998, **69**, 607.

32 J. S. Murray, J. M. Seminario, P. Politzer and P. Sjoberg, *Int. J. Quantum Chem.*, 1990, **38**, 645.

33 A. K. Ghose, V. N. Viswanadhan and J. J. Wendoloski, Prediction of hydrophobic (lipophilic) properties of small organic molecules using fragmental methods: an analysis of ALOGP and CLOGP methods, *J. Phys. Chem. A*, 1998, **102**, 3762.

34 I. Ledeți, G. Vlase, T. Vlase, A. Fuliaș and L.-M. Șuta, *J. Therm. Anal. Calorim.*, 2015, DOI: 10.1007/s10973-015-5071-5.

35 H. Carrer, J. Cortez, L. M. Frare, M. B. Costa and P. R. S. Bittencourt, *J. Therm. Anal. Calorim.*, 2016, **123**, 927.

36 S. Clède, F. Lambert, R. Saint-Fort, M. A. Plamont, H. Bertrand, A. Vessières and C. Policar, *Chem. – Eur. J.*, 2014, **20**, 8714.

37 A. Ganguly, P. Chakraborty, K. Banerjee and S. K. Choudhuri, *Eur. J. Pharm. Sci.*, 2014, **51**, 96.

38 S. Meker, K. Margulis-Goshen, E. Weiss, O. Braitbard, J. Hochman, S. Magdassi and E. Y. Tshuva, *ChemMedChem*, 2014, **9**, 1294.

39 A. A. Stavrovskaya, *Biochemistry*, 2000, **65**, 95 (translated from Biokhimiya, 2000, 65, 112).

40 G.-Y. Liou and P. Storz, *Free Radical Res.*, 2010, **44**, 479.